

# We are IntechOpen, the world's leading publisher of Open Access books Built by scientists, for scientists

6,900

Open access books available

186,000

International authors and editors

200M

Downloads

Our authors are among the

154

Countries delivered to

TOP 1%

most cited scientists

12.2%

Contributors from top 500 universities



WEB OF SCIENCE™

Selection of our books indexed in the Book Citation Index  
in Web of Science™ Core Collection (BKCI)

Interested in publishing with us?  
Contact [book.department@intechopen.com](mailto:book.department@intechopen.com)

Numbers displayed above are based on latest data collected.  
For more information visit [www.intechopen.com](http://www.intechopen.com)



# UV-Vis Photodetector with Silicon Nanoparticles

J.A. Luna-López<sup>1</sup>, M. Aceves-Mijares<sup>2</sup>, J. Carrillo-López<sup>1</sup>,  
A. Morales-Sánchez<sup>3</sup>, F. Flores-Gracia<sup>1</sup> and D.E. Vázquez Valerdi<sup>1</sup>

<sup>1</sup>*Science Institute-Research Center for Semiconductor Devices-Autonomous  
Benemérita University of Puebla*

<sup>2</sup>*Department of Electronics, National Institute of Astrophysics,  
Optics and Electronics INAOE*

<sup>3</sup>*Centro de Investigación en Materiales Avanzados S. C.,  
Unidad Monterrey-PIIT, Apodaca, Nuevo León,  
México*

## 1. Introduction

Nowadays, photodetector devices are important components for optoelectronic integration. In the past, various photodetector structures have been developed from pn junction, pin diode, bipolar transistor, avalanche photodiodes (APD), and metal-semiconductor-metal (MSM) structures (Ashkan et al., 2008; Hwang & Lin, 2005; DiMaria et al., 1984a, 1984b; Sabnis et al., 2005; Foster et al., 2006). In these structures, different semiconductors such as Si, III-V and II-VI compounds have been used, depending on the wavelength range to be detected. Nevertheless, silicon is the most common and important semiconductor in the integrated circuit technology, but it has an indirect band gap inhibiting optical functions. Silicon sensors are usually used in the visible-to near infrared (VIS-NIR) range. However, some commercial Si sensors have been enhanced to detect in the ultraviolet (UV) range, but they have one or more of the following weaknesses: very expensive, reduced responsivity in the VIS-NIR range, lack of compatibility with IC processes and a complex technology. So, most of the available materials for UV detection are not silicon but compound semiconductors (Hwang & Lin, 2005). Then, many works have been done to study Si-based optoelectronics materials to overcome the drawback of silicon. Silicon rich oxide (SRO) is one of such materials. SRO is a variation of silicon oxide, in which the content of silicon is changed. The main characteristic to enhance the UV detection in this material is the formation of silicon nanostructures. Among the different techniques to synthesize Si-nps in SRO films, the low pressure chemical vapour deposition (LPCVD) technique offers the films with the best luminescence properties, compared with those obtained by plasma enhanced CVD and silicon implantation into SiO<sub>2</sub> films (Morales et al., 2007).

The optical and electrical properties of SRO-LPCVD films have been extensively studied as a function of the silicon excess, temperature and time of thermal annealing (Morales et al., 2007; Zhenrui et al., 2008). Silicon nanoparticles (Si-nps) with different sizes in SRO-LPCVD films have been observed by transmission electron microscope (TEM) technique (Luna et al., 2009). Depending on the excess of Si content, SRO possesses some special properties such as charge trapping, carrier conduction and luminescence. Some novel devices have been

proposed using these properties (Zhenrui et al., 2008, Luna et al., 2006, Berman et al., 2008). In Luna et al., 2006, a photodetector using SRO and an induced PN junction were presented, and it was shown that even when the active area is covered by opaque aluminium the photocurrent is considerable. However, it is not clear the reason of such a high response. Also, Aceves et al. proposed (Aceves et al., 1999) that an induced pn junction could be used as a photodetector and that if high resistivity silicon is used a high photoresponse could be expected. However, this idea has not been corroborated.

In this chapter, optical properties as absorption coefficient and optical band gap of SRO with Si-nps and different silicon excess were also studied in order to be able to apply them in optical photodetectors. A photodetector made of a simple Al/SRO/Si MOS-like grid structure is reported. The devices fabricated on high resistivity substrate possess high responsivity in photodetection from UV to VIS-NIR radiation. This structure requires few fabrication process steps and is completely compatible with the complementary metal-oxide-semiconductor (CMOS) technology. The possible mechanisms involved in the light detection and the extended photosensitivity of this structure are analysed and discussed.

## 2. Experimental procedure

The experimental procedure is divided in two parts. The first part is the following: SRO films were deposited on silicon substrates in a horizontal LPCVD hot-wall reactor using nitrous oxide ( $\text{N}_2\text{O}$ ) and silane ( $\text{SiH}_4$ ) as the reactant gases at  $700^\circ\text{C}$ . The partial pressure ratios  $R_o = [\text{N}_2\text{O}]/[\text{SiH}_4]$ , were  $R_o = 10, 20$ , and  $30$ . The thicknesses of the SRO films were about  $500\text{ nm}$ . Silicon Excess in these films are about  $12.7, 8.0$  and  $5.5\text{ at.}\%$  for  $R_o = 10, 20$  and  $30$ , respectively (Luna et al., 2007). After deposition, the films were densified at  $1000^\circ\text{C}$  for 30 minutes in nitrogen atmosphere, and then some of them were thermally annealed at  $1100^\circ\text{C}$  for 180 minutes in nitrogen atmosphere.

The XRD measurements were done using a Bruker AXS D8 Discover diffractometer with  $\text{Cu K}\alpha$  radiation. The surface morphology of SRO films was studied using a nanosurf easy Scan AFM system version 2.3, operated in contact mode. A  $4 \times 4\text{ }\mu\text{m}^2$  scanned area was used for each topographic image, and a  $450\text{-}\mu\text{m}$ -long single-crystal Si cantilever operated at  $12\text{ kHz}$  (type vista probes CL contact mode AFM probes) was used. Five different scans were done for each sample, showing good reproducibility. AFM images were analysed using scanning probe image processor (SPIP) software (Jogensen, 2002).

For TEM measurements, an energy-filtered TEM (EFTEM) was used. The images were obtained using an electronic microscope (JEOL JEM 2010F); all the EFTEM images were measured using a Si plasmon of  $17\text{ eV}$  and cross-section views. EFTEM enables us to detect amorphous Si nanoclusters embedded in an oxide matrix (Spinella et al, 2005). Also, an FEI Tecnai F30 high-resolution TEM (HRTEM) with acceleration voltage of  $300\text{ kV}$  and line resolution of  $0.2\text{ nm}$  was used to study the microstructure of the Si nanocrystals.

Room-temperature photoluminescence (PL) of the SRO films was measured using a Perkin-Elmer spectrometer LS-50B model with a xenon source and a monochromator. The samples were excited using  $250\text{-nm}$  radiation, and the emission signal was collected from  $400$  to  $900\text{ nm}$  with a resolution of  $2.5\text{ nm}$ . A cut-off filter above  $430\text{ nm}$  was used to block the light scattered from the source.

Optical transmittance measurements were made in the UV range to near infrared at room temperature, using a spectrophotometer Perkin-Elmer LMBD 3B UV/VIS.

In the second part of the experimental procedure SRO films were deposited on n-type Silicon (100) substrates with resistivity of 2000-5000  $\Omega$ -cm and with a N+ implanted region on the back side. SRO layers were deposited in a horizontal LPCVD hot wall reactor using SiH<sub>4</sub> (silane) and N<sub>2</sub>O (nitrous oxide) as reactive gases at 700 °C. The gas flow ratio Ro was used to control the amount of silicon excess in the SRO films. Ro = 10, 20, and 30, corresponding to a silicon excess from 12 to 5 %, were used for this experiment. After deposition, the samples were thermally annealed at 1000° C in N<sub>2</sub> atmosphere for 30 minutes. Aluminium grids with area of A = 0.073 cm<sup>2</sup> were patterned on the SRO surface by evaporation and standard photo-lithography. Figures 1(a) and 1(b) show a cross-section view scheme, with an approximation at only 3 grid electrodes and an image of the surface of the fabricated devices. The surface Al grid electrodes have several fingers with 40  $\mu$ m width and distanced at 205  $\mu$ m, as observed in figure 1(b). It is important to remark that the zones between fingers are covered by the SRO film.

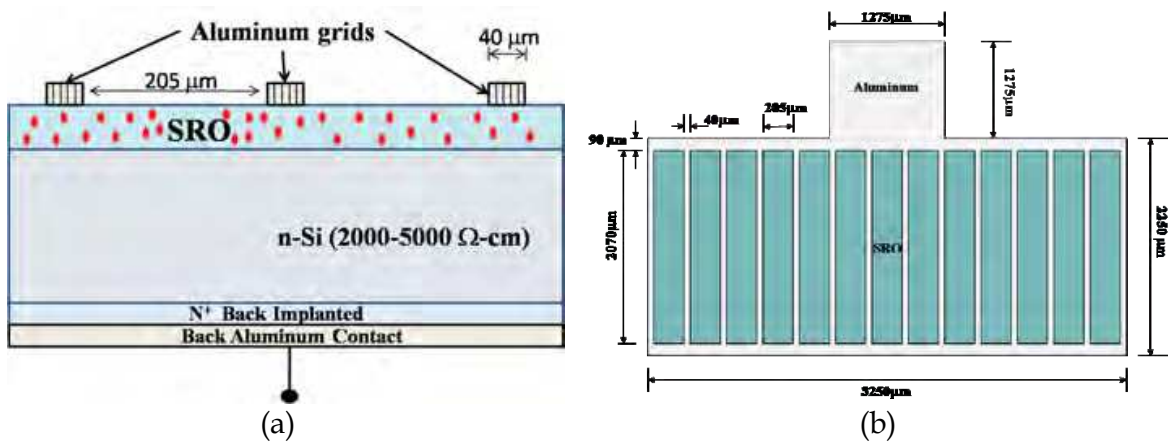


Fig. 1. Scheme of the Al/SRO/Si MOS-like device, (a) a cross-section view scheme of the fabricated devices with an approximation at only 3 grid electrodes and (b) dimensions of a device and of the grids electrodes.

Ellipsometric measurements were made with a Gaertner L117 ellipsometer to obtain the thickness and refractive index of the SRO films before annealing, whose values are shown in Table 1.

Ro	Refractive index	Thickness (Å)
10	1.78 ± 0.01	720 ± 28
20	1.55 ± 0.03	755 ± 25
30	1.46 ± 0.01	591 ± 3

Table 1. Refractive index and thickness of SRO films.

Current versus voltage (I-V) measurements were performed at room temperature, illuminated with UV or white light and under dark conditions, using a computer controlled Keithley 6517A electrometer. The voltage sweep was done with a rate of 0.1 V/s. Illumination was performed with an UV lamp (UVG-54, 5 to 6 eV approximated range) and a white light lamp (1.7 to 4 eV approximated range) with an output power of 4.3 mW/cm<sup>2</sup> and 3.2 mW/cm<sup>2</sup>, respectively. The power of lamps was measured using a radiometer (International Light, USA. IL1 400A). On the other hand, other current versus voltage (I-V)

measurements were performed at room temperature using a computer controlled Keithley 236 source-meter, under illuminations at specific wavelengths of 400, 650 and 1000 nm conditions, with a Sciencetech 9040 monochromator. The measured power were 83.6  $\mu\text{W}/\text{cm}^2$ , 238.9  $\mu\text{W}/\text{cm}^2$  and 11.5  $\mu\text{W}/\text{cm}^2$  for 400, 650, 1000 nm wavelengths, respectively.

3. Results

3.1 Structural, optics and photoelectric results

Figure 2 shows the XRD patterns of SRO films with  $R_o = 10$  and 20, annealed at 1100 °C for 180 minutes on silicon substrate. Peaks at 21, 28.5° and 47.4° are observed for SRO films with  $R_o = 10$  and they are ascribed to  $\text{SiO}_2$ , Si (111) and (220), respectively. However, those peaks at 28.5° and 47.4° disappeared for  $R_o = 20$ . As  $R_o$  becomes higher ( $R_o = 30$ ), the diffraction peaks were not observed (not shown here).

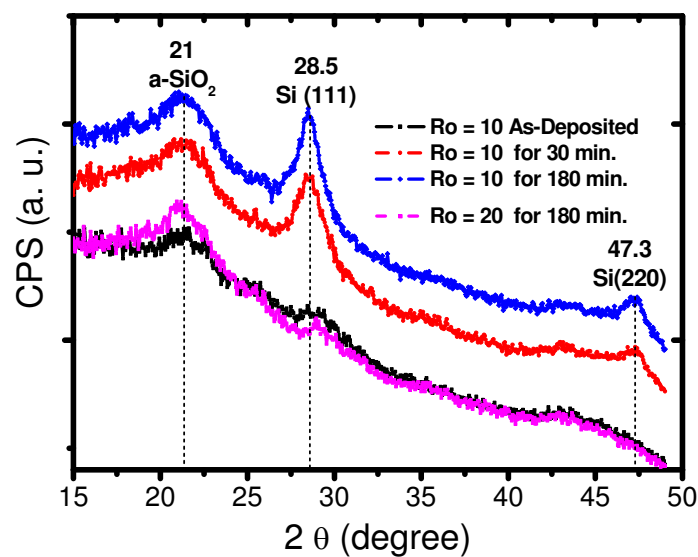


Fig. 2. XRD patterns of SRO films with  $R_o = 10$  and 20 annealed at 1100 °C for 180 minutes on silicon substrate.

The average crystal size ( $D$ ), dislocation density ( $\delta$ ) and microtension ( $\epsilon$ ) of the silicon nanocrystals (Si-ncs) for  $R_o = 10$  were estimated from the Si (111) peak using the Scherrer formula (Karunakaran, B., et al., 2002, Comedi,D., et al., 2006,) and are listed in Table 2.  $\delta$  and  $\epsilon$  decreased when the annealing time increases for  $\text{SRO}_{10}$  films, which is related to a reduction on the defect concentration and imperfections of the nanocrystal cell (Yu et al, 2006).

Samples of SRO on silicon					
SRO films	$2\theta$ (°)	[hkl]	( $D$ ) (nm)	$\delta$ ( $10^{12} \text{ cm}^{-2}$ )	$\epsilon$ ( $10^{-3}$ )
10TT30	28.65	Si [111]	4.6	4.6	8.0
10TT180	28.55	Si [111]	5.4	3.4	7.0
20TT180	29.1	Si [111]	2.8	12.2	13.0

Table 2. Structural parameters of the SRO Films obtained from the XRD measurements for Si (111) peak.



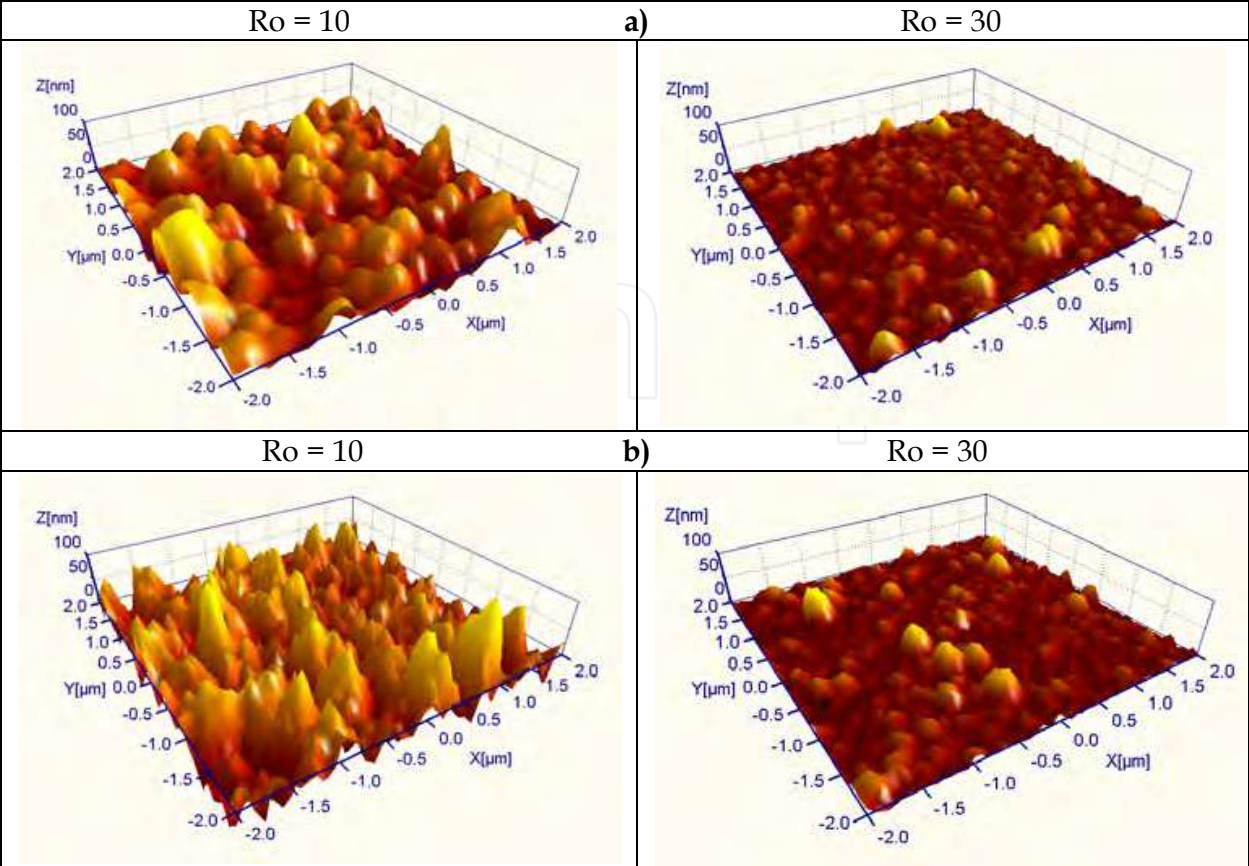


Fig. 3. 3D AFM images of a) as-deposited and b) thermally annealed at 1100 °C SRO<sub>10</sub> and SRO<sub>30</sub> films on silicon. Scanned area: 4 × 4 μm<sup>2</sup>.

Figure 4 shows a comparison of the average roughness <Sa> for the SRO films with different Si excess for as-deposited, densified and annealed films.

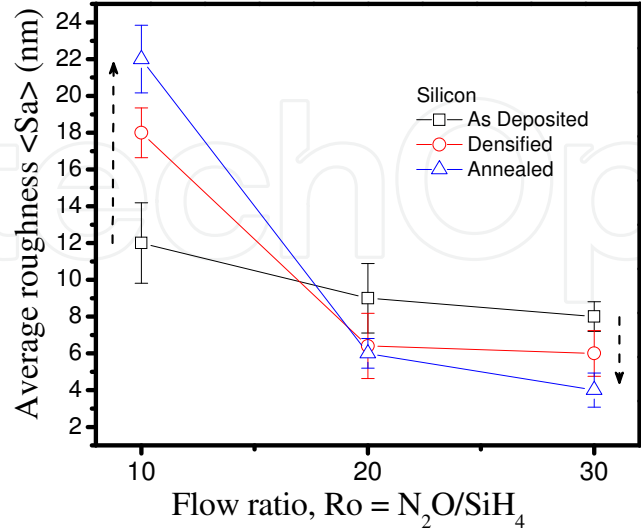


Fig. 4. Average roughness <Sa> as a function of the flow ratio (Ro) for as-deposited, densified, and thermally annealed SRO films deposited on silicon (lines are plotted as an eye-guide). Scanned area: 4 × 4 μm<sup>2</sup>.

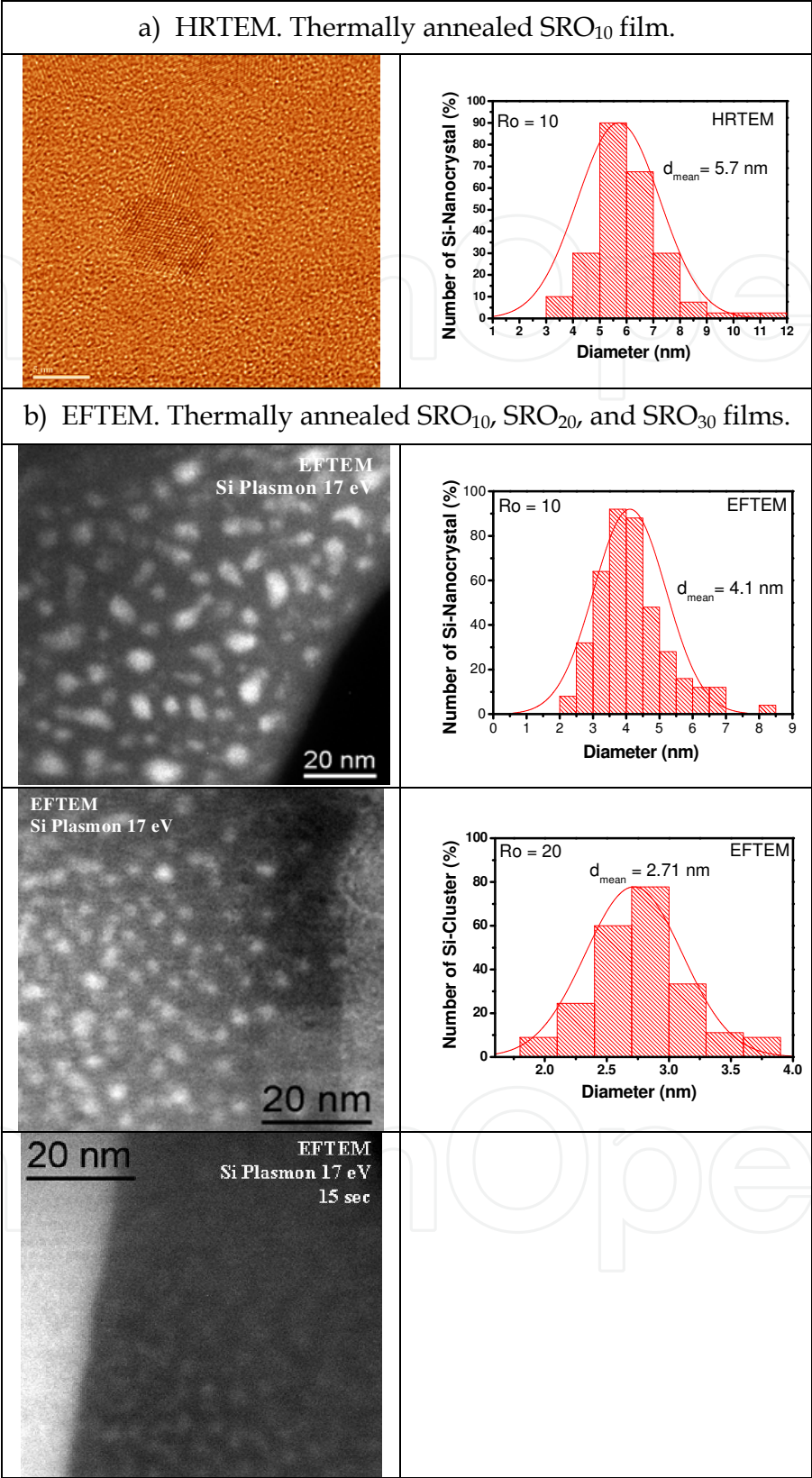


Fig. 5. Silicon nanocrystals in SRO<sub>10</sub> films and silicon clusters in SRO<sub>10</sub>, SRO<sub>20</sub>, and SRO<sub>30</sub> films were observed by a) HRTEM and b) EFTEM, respectively, after thermal annealing at 1100 °C.

Figure 3 displays three-dimensional (3D) AFM images of as-deposited and thermally annealed SRO films with different excess silicon. All images exhibit a rough surface. For as-deposited SRO films, the roughness decreases with increasing  $R_o$ , as shown in Fig. 3 (a). After thermal annealing, roughness increased for SRO films with  $R_o = 10$ , as depicted in Fig. 3 (b); for  $R_o = 20$  and 30, no significant influence is visible from 3D images.

Figure 5 shows the HRTEM and EFTEM images of the annealed SRO films. For  $R_o=10$ , HRTEM and EFTEM images clearly show Si nanocrystals (Si-ncs) with a mean size of  $\sim 5.7$  nm, as seen in Figures 5 (a) and 5 (b). Si-ncs were not observed for  $R_o = 20$  and 30. However, bright zones associated with amorphous silicon clusters were observed by EFTEM on SRO films with  $R_o = 20$  and 30, as shown in Fig. 5 (b). Si clusters with a mean size of  $\sim 2.7$  nm were observed for  $R_o = 20$ , whereas for  $R_o = 30$ , because of low contrast and sharpness, the shape was not very clear, but Si clusters with size  $\leq 1$  nm could be identified.

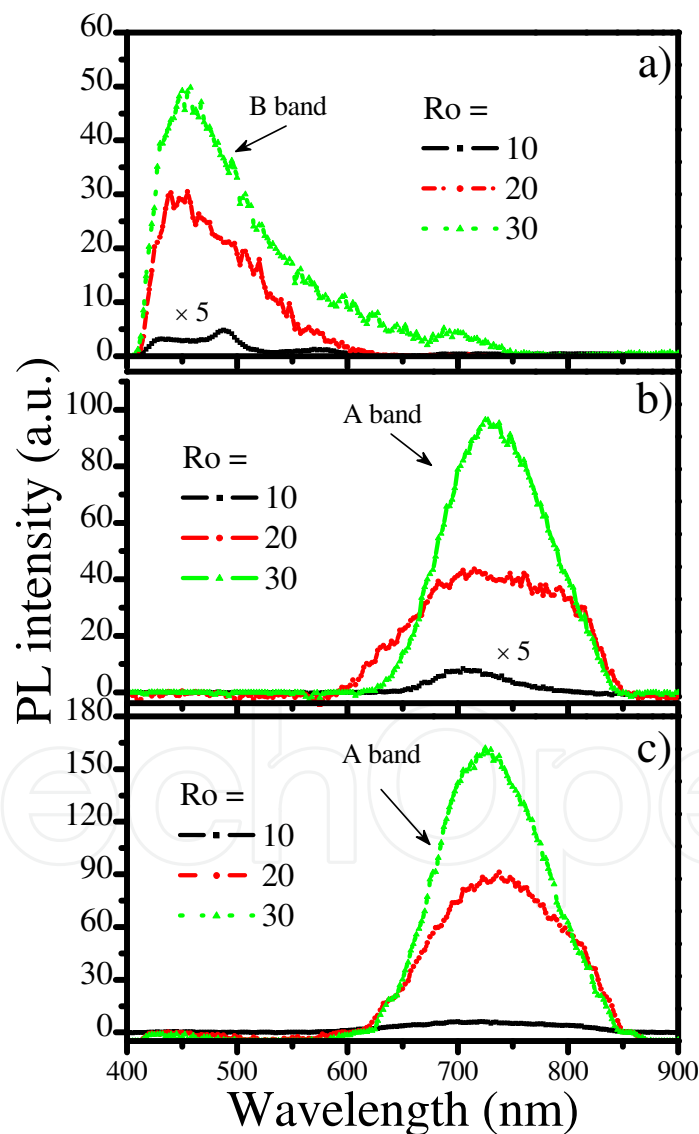


Fig. 6. PL spectra of SRO films with  $R_o = 10, 20$  and  $30$  and a) as- deposited, b) densified at  $1000^\circ\text{C}$  for  $30$  min, and c) thermally annealed at  $1100^\circ\text{C}$  for  $180$  minutes deposited on silicon substrate.



Figures 6 (a)–6 (c) show the PL spectra of the as-deposited, densified, and annealed SRO films, respectively. Two PL bands can be observed: B band (400–600 nm) and A band (600–850 nm). For as-deposited SRO films, the intensity of the B band increases with  $R_o$ , as shown in Fig. 6 (a). After densification, the B band disappears and the A band becomes visible [see Fig. 6 (b)]; prolonged annealing at higher temperature of 1100 °C for 180 min enhanced its intensity, as shown in Fig. 6 (c). SRO films with large  $R_o$  (low excess Si) always show higher PL intensity. On the other hand, the PL peak position did not show any significant shift with  $R_o$ .

Transmittance spectra were measured to obtain the optical band gap of SRO films. Transmittance spectra for  $R_o = 10, 20$  and  $30$  films deposited on sapphire are shown in Figure 7. As can be observed, the transmittance of all these films is relatively high ( $> 80\%$ ) between 600 and 900 nm, and reduces to zero for wavelengths below 600 nm. The annealing time does not produce a clear variation; however, the  $R_o$  causes a clear shift of the curves towards lower wavelengths. These samples have different behaviours, in agreement with the  $R_o$  value and annealing time.

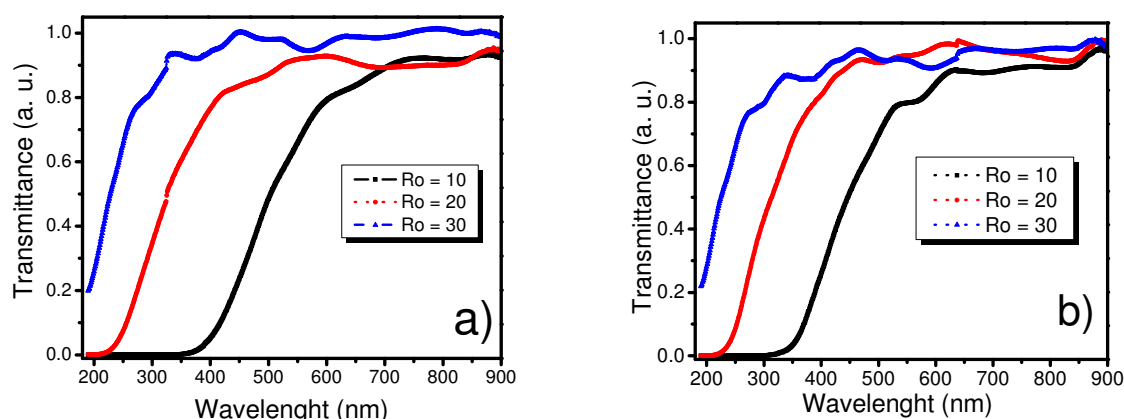


Fig. 7. UV/Vis transmittance spectra for  $R_o = 10, 20$ , and  $30$  on sapphires substrates. a) densified at 1000 °C and b) annealed at 1100 °C.

The absorption coefficients were determined from transmission spectra of Figure 7, and they are shown in Figure 8. The absorption coefficients show different behaviour with the  $R_o$  values.

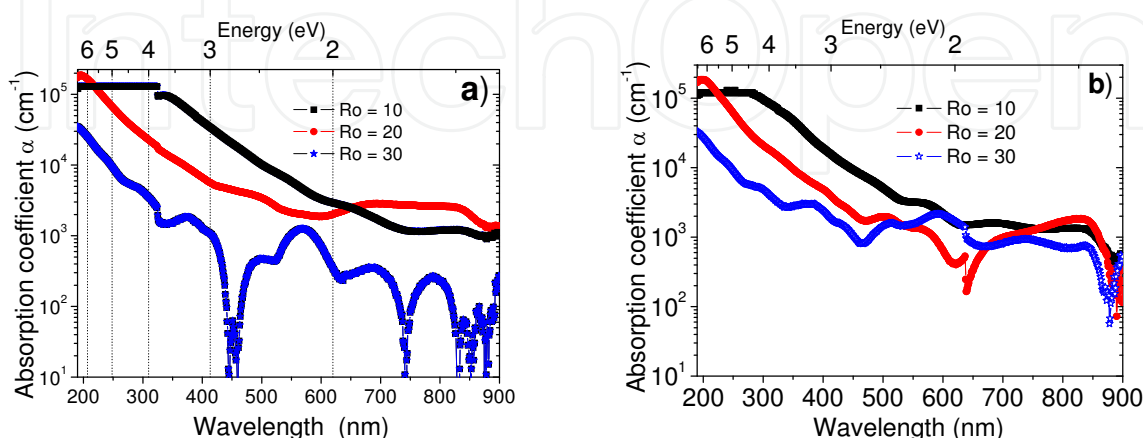


Fig. 8. Absorption coefficients in the range of the U-V to NIR for a) densified and b) thermally annealed SRO films.

The fundamental absorption edge in most semiconductors follows an exponential law (Pankove, 1975). The absorption coefficient  $\alpha$  is correlated with the transmittance  $T$  and the reflectance  $R$  of a sample with thickness  $d$  through the relation:

$$T \approx (1 - R)^2 e^{-\alpha d}$$

(1)

The absorption coefficient  $\alpha$  shown in Figure 8 was estimated as:

$$\alpha(\hbar\nu) = \frac{-\ln(T(\hbar\nu))}{d}$$

(2)

From the Tauc law:

$$(\alpha\hbar\nu)^{1/2} \propto (\hbar\nu - E_g)$$

(3)

Graphs of  $(\alpha\hbar\nu)^{1/2}$  versus photon energy ( $\hbar\nu$ ) and the corresponding optical band gap are shown in Figure 9.

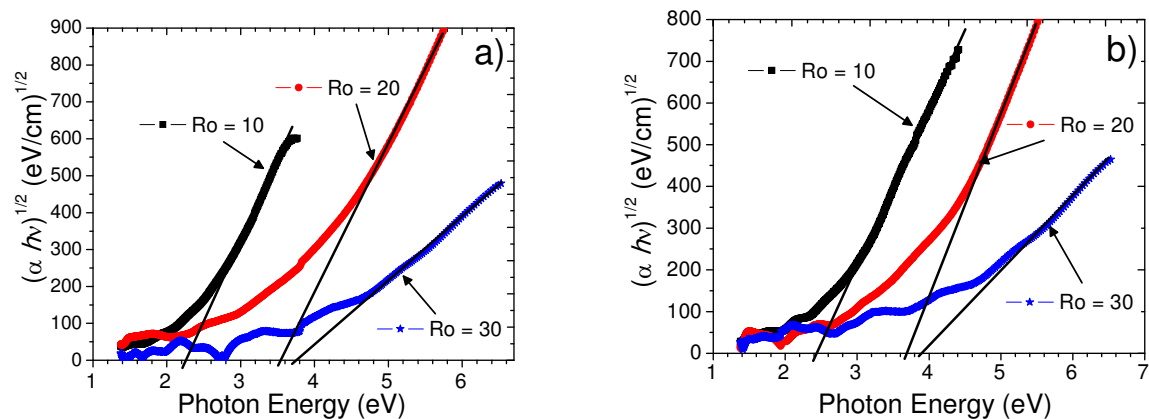


Fig. 9.  $(\alpha\hbar\nu)^{1/2}$  vs. photon energy a) densified and b) thermally annealed SRO films with different  $R_o$ . Straight lines are used to estimate the optical band gap.

It is observed that the position of the absorption edge moves towards higher energy when  $R_o$  increases. The values obtained for the optical band gap are listed in Table 3.

Ro	Band gap ( $E_g$ )			
	Densified (1000°C)	Annealed at 1100°C		
		30 min	60 min	180 min
10	2.28±0.04	2.4±0.04	2.4±0.02	2.43±0.04
20	3.52±0.03	3.57±0.03	3.6 ±0.06	3.69 ±0.03
30	3.76 ±0.07	3.73 ±0.06	3.86±0.04	3.89±0.04

Table 3. Energy of the optical bang gap obtained from the Tauc’s method for SRO films with different  $R_o$  values and times of thermal treatment.

The optical band gap increases with  $R_o$ . In this case, as the silicon excess reduces the absorption coefficient also reduces, as shown in Figure 8. As  $R_o$  moves towards low values,

the band gap moves towards that of the bulk silicon; consequently, it is expected that the properties of an indirect semiconductor be kept.

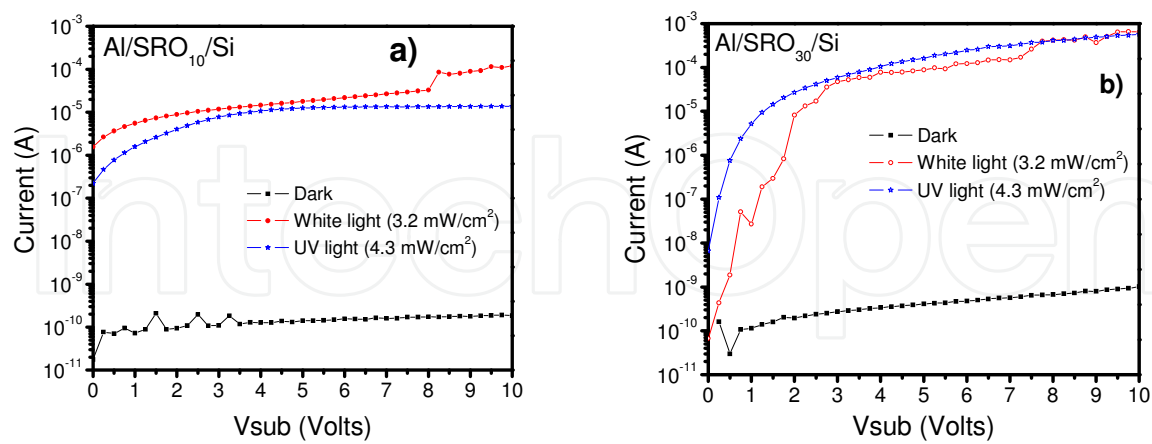


Fig. 10. I-V curves of the Al/SRO/Si MOS-like grid structure for a) SRO<sub>10</sub> and b) SRO<sub>30</sub> under dark and illumination conditions.

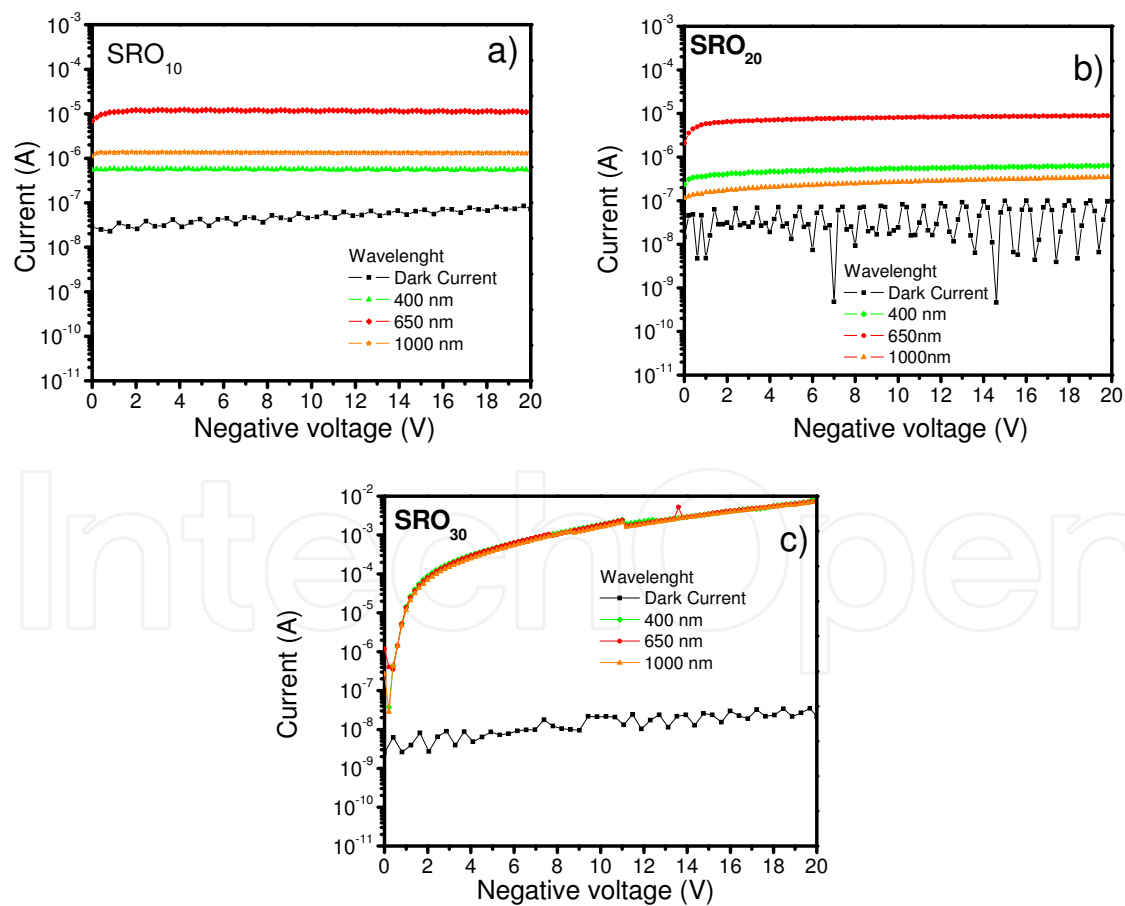


Fig. 11. Current-voltage characteristics of the Al/SRO/n-Si MOS-like structures with a) SRO<sub>10</sub>, b) SRO<sub>20</sub>, and c) SRO<sub>30</sub> films under dark and illuminated with 250, 400, 650, 1000 nm wavelengths.

MOS-like structures were fabricated and measured. Figures 10(a) and 10(b) show, respectively, the typical I-V characteristics of devices with  $R_o = 10$  and 30 at the surface inversion condition (negative voltage at the gate respect to the substrate), in dark and under UV and white light illumination. The dark current is on the order of  $10^{-10}$  A, indicating a low leakage current in these structures. However, a large photocurrent was obtained when the structures were illuminated, this fact indicative of a high optical sensitivity in this simple structure. Similar photo-response was obtained with structures made with SRO of  $R_o = 20$ .

I-V characteristics of devices with  $R_o = 10$ , 20 and 30 at the surface inversion condition and under illumination at specific wavelengths are shown in Figures 11(a), 11(b) and 11(c), respectively. The order of the dark current is  $10^{-8}$  A indicating a low leakage current in these structures. This current value changed from that obtained in Figure 10 because of the fact that different devices were measured and these ones have a bigger dark current. Nevertheless, at both cases a large photocurrent was obtained when the structures were illuminated. Therefore, these simple structures show high optical sensitivity. Different photocurrents were obtained for the different  $R_o$ 's in each wavelength, being the SRO structures with  $R_o = 30$  which have the highest photo-response.

#### 4. Analysis and discussion

The results show that SRO films properties depend on the silicon excess and the annealing conditions. XRD results showed that in SRO films with thermal annealing, diffusion of the silicon excess took place creating silicon nanoparticles indicated mainly by the peaks, and their size depends upon the silicon excess in the SRO films. Diffractograms on Figure 2 show crystalline orientations (111), (220) and (311) of the nc-Si. It is clear that, when the silicon excess is higher, the agglomerated Si is present and with thermal annealing the generation of nc-Si is obtained, the diffusion coefficient of Si in the SRO at 1100 °C was calculated as  $\sim 1 \times 10^{-16} \text{ cm}^2\text{s}^{-1}$ . Diffraction peaks indicate the formation of nc-Si and it should be interpreted as a phase separation between nc-Si and  $\text{SiO}_2$  induced by thermal annealing.

Si-ncs sizes obtained by XRD are similar to those observed by HRTEM and EFTEM. For  $R_o = 10$ , HRTEM images clearly show Si-ncs with a mean size of 5.7 nm but Si-ncs were not observed for  $R_o = 20$  and 30. However, bright zones associated with amorphous silicon clusters were observed by EFTEM on SRO films with  $R_o = 20$  and 30. Si clusters with a mean size of 2.7 nm were observed for  $R_o = 20$ , whereas for  $R_o = 30$  the shape was not very clear, because of low contrast and sharpness, but Si clusters with 1 nm size could be identified.

AFM images of the SRO films on silicon substrates show that the shape and size of the roughness change with  $R_o$ . For SRO films with  $R_o = 10$ , the roughness increased after thermal annealing. However, for SRO with  $R_o = 20$  and 30, the roughness reduced, as shown in Figure 4. For  $R_o = 10$  the roughness can be as high as a maximum of 24 nm. However, for  $R_o = 30$  the surface looks smooth and the maximum height is about 5 nm. Then, for  $R_o = 10$ , the roughness observed through AFM can be associated to Si-ncs. Nevertheless, for SRO films with  $R_o = 20$  and 30 the roughness observed can be ascribed to

silicon compounds, or silicon clusters, rather than to Si-ncs. Therefore, elemental Si, SiO<sub>x</sub>, and SiO<sub>2</sub> phases separate after annealing, and depending on the silicon excess, one of those phases can be dominant.

Si clusters in the SRO films are produced by diffusion of the Si excess at high temperature. That is, when SRO is annealed, the silicon particles diffuse creating silicon agglomerates around a nucleation site. If the Si excess is high enough, the Si clusters will be crystallized forming Si-ncs. However, when the Si excess reduces, Si clusters are amorphous due to the large lattice mismatch between SiO<sub>2</sub> and Si. If the Si excess is low enough, there are no pure Si clusters created, instead, Si-O compounds are formed in SRO films. Then a more homogeneous material is obtained. Of course, these two mechanisms are not exclusive each other, and they can exist simultaneously. However, one of them will dominate depending on the silicon excess.

On the other hand, there are different factors that have an important impact on the optical properties of the SRO films. Therefore, it is necessary to understand these factors for designing materials to be used in photodetectors. In our case, factors such as substrate type, silicon excess, annealing temperature and composition are very important for the optical properties of SRO films. PL also depends on Ro and thermal-annealing conditions. In Figure 6, all the as-deposited SRO films show a weak PL band at 400–600 nm (B band). After thermal annealing, the B band disappears and another PL band (A band) dominates. The intensity of the A band increases with the time and annealing temperature. The PL property of SRO has been extensively studied in literature. Two major mechanisms for PL in this kind of materials are generally accepted: quantum confinement effects in the Si-ncs and defect-related effects. In our samples, intense PL (A band) in SRO<sub>30</sub> was observed; however, SRO<sub>30</sub> has silicon compounds rather than Si-ncs. Therefore, the A band cannot be associated with quantum confinement effects; instead, it should be associated with Si-related defects. As reported previously (Lee et al., 1979, Lin et al., 2005), the B band is also associated with F and E defects and different types of oxygen vacancies. Although there are many reports about the origin of PL, most of them relates PL with the bulk microstructures of SRO. A very few studies report on the correlation between the PL and the surface morphology of the SRO films. Other authors (Torchynska et al, 2002) have reported that the diameter and area of the grains on the porous silicon film surface have an important influence on the PL spectra. In our case, SRO is not porous Si but it is considered to be Si nanoclusters embedded in an oxide matrix with very stable optical and electrical properties—quite different than porous silicon. However, from AFM images, the surface is completely irregular, with bumps of different heights and shapes. So, these bumps can be treated as grains on the surface. The grains vary in size depending on the Ro value and annealing time. They can then be related to the emission, as it was done for porous silicon. The height of the roughness, equivalently to the height of the grains, was already related to the silicon cluster size (Luna et al, 2007).

It is observed that the main influence on the structural and optical properties is due to the Ro value of the SRO films, their thickness, annealing time and substrate type. In XRD and AFM measurements important changes in the structure were observed, which indicates that the substrate has influence on the structural properties of the deposited SRO films. In the PL spectra the unusual high intensity of the A band is remarkable. The explanation for this observation is that different oxidation mechanisms lead to different termination of the tetrahedron SiO<sub>4</sub> and Si<sub>4</sub> of the silicon oxide and silicon, respectively. Si can be terminated



with different combinations of  $\text{Si-Si}_{4-n}\text{O}_n$  compounds (with  $n = 0$  to  $4$ ), it can be terminated by double bond to an oxygen atom ( $\text{Si=O}$ ), oxygen vacancies or by a bond to a hydroxyl group ( $\text{Si-O-H}$ ).

Taking these results into account, it seems that the types of radiative centres producing the luminescence in SRO films deposited on silicon substrate are similar in the A band, but different in the B band. Therefore, depending on the substrate type, specific structural defects are formed in the SRO films. The Si content in the SRO system to form the phase (crystalline or amorphous) and the structure (crystal size and morphology) of the Si-nps, and especially of their surrounding Si-SiO<sub>2</sub> interface, has significant influence on the optical properties. Also, the optical band gap tends towards the optical band gap of the Bulk silicon by increasing the silicon excess, and with a lower silicon excess the optical band gap will tend towards that of the SiO<sub>2</sub>.

The large variety of factors that can be used to influence the structural and optical properties makes these materials very interesting for optoelectronics applications. A shift of the optical band gap is possible by varying the silicon excess. Also, the PL emission can be tuned by thermal annealing, silicon excess and substrate type.

Therefore, MOS-like structures were designed to obtain high photocurrent. The results show that Al/SRO/Si grid structures have high photocurrent at different wavelengths. The large photocurrent is due to the photocarriers generation in the SRO films and also in the Si substrate. The mechanism of the carrier transport in the SRO layers can be via tunneling (Yu et al, 2008). High density of Si-nps and defects in the SRO films create conduction paths and then the photogenerated carriers can move through them allowing a large photocurrent.

This simple structure presents high optical sensitivity for UV and the visible to near infrared range (from 250 nm to 1000 nm), as depicted in Figures 10 and 11. The UV response of the SRO layer has been demonstrated in different reports, apparently the silicon nanoparticles (embedded or not) are in some way sensible to the UV. In (Nayfeh et al, 2004) the authors use silicon nanocrystals (not embedded) to develop an UV sensor in the 250 nm to 350 nm range. Also, our group has developed an UV-Vis-NIR sensor using SRO (with embedded Si nps) (Berman et al., 2008). Moreover, it is well known that red emission is obtained when SRO is irradiated with UV. So, UV response of the SRO could cooperate in two ways to the observed response of the devices reported in this work. First, the red photoluminescence produced by the SRO impinges into the silicon, which has a high sensitivity to these wavelengths. Second, the SRO itself has demonstrated some conduction properties under illumination, so this current component could be added to the photocurrent (Luna et al, 2010).

Now, the high photoresponse can only be explained if the whole device is considered photosensible. That includes the components due to the SRO (already discussed), and the components in the silicon. As Figure 12 shows, there are two zones in the silicon substrate where the light could produce electron-hole pairs (EHP): (1) under the Al fingers and (2) in the exposed regions between the fingers. Due to the bias of the device, under the Al fingers the silicon surface is in inversion (layers of holes formed), forming an induced-PN junction. However, owing to the fact that this PN junction is covered by an opaque Al layer, very few photons will produce photocurrent; then the current component due to this layer should be

small. So, the PN junctions could act as a collector of the minority carrier produced somewhere else, and then contribute to the photocurrent through the SRO that allows the electrons to move from the substrate to the Al electrode.

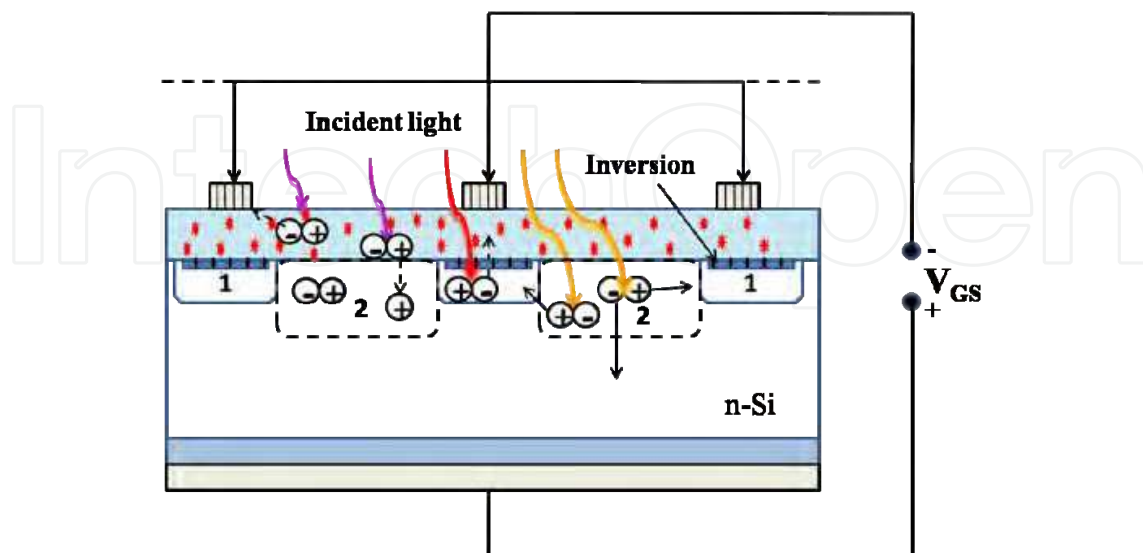


Fig. 12. A cross-section scheme of the zones in the SRO films and silicon high resistivity substrate where the light could produce electron hole-pairs (EHP). (1) Under the Al fingers the silicon surface is in inversion due to the bias of the device, in this case only a few photons arrive to the edge of the region, and (2) in the SRO films in the Al uncover between the fingers. The dash lines marks the maximum length where a photon can reach.

On the other hand, the SRO traps charge both positive and negative, so that the surface in this zone could be in accumulation if the SRO is positively charged, in inversion if the SRO is negatively charged, or neutral if there is no charge in the SRO. The resistivity of the silicon substrates used for this experiment is 2000-5000 ohms-cm, so small quantities of trapped charge could bias the surface. Moreover, the charge could get to be trapped during the fabrication process, especially during the high temperature process.

The inversion or accumulation of the surface produces channels where the carriers could move toward the fingered zone where they contribute to the photocurrent. However, in our devices the dark current is very low ( $< 10^{-8}$  A) meaning that the channels do not exist.

Then, the only possibility to increase so much the photocurrent is that the uncovered neutral region under illumination produces electron-hole pairs able to arrive at the Al covered area. As known, only the EHP produced within a diffusion length,  $L = \sqrt{D\tau}$  ( $D$  is the diffusivity and  $\tau$  is the lifetime), will arrive at the PN junctions. In this case, only the holes which are the minority carriers are significant. The diffusivity can be estimated from the mobility using the Einstein's relationship. Also, the resistivity of the silicon substrate used here is very high and the mobility ( $510 \text{ cm}^2/\text{Vs}$ ) does not vary much for resistivities greater than  $100 \text{ } \Omega\text{-cm}$  (Cronmeyer, 1957). Therefore, a conservative value of the diffusivity is  $13.184 \text{ cm}^2/\text{s}$  (Grove, 1967). Härkönen et al. (Härkönen et al., 2006) studied the lifetime of high resistivity silicon under low and high injection levels of carriers. They found that for high resistivity silicon the recombination lifetime is longer than 1 ms. Just for reference in our

group, generation lifetime of high resistivity silicon was estimated to be between 1 and 2 ms (Luna et al., 2005). Then, a value of diffusion of 0.114 cm, or 1140  $\mu\text{m}$  is calculated.

Now, for UV radiation (200 - 300 nm) the absorption coefficient is approximately,  $1 \times 10^6 \text{ cm}^{-1}$ , and the absorption depth is 0.01  $\mu\text{m}$  (Sze, 2006). For other wavelengths, for example around 600 nm, the absorption depth is about 5  $\mu\text{m}$ . In spite of fact that the absorption is quite superficial for UV, most of the generated holes reach the induced PN junctions due to their long diffusion length, and in general this is true for all the detection range: UV-Vis-NIR. So, the high sensitivity observed in this device is due to a large silicon volume where all the generated carriers contribute to the photocurrent and, as a complement, some photo-effects in the SRO also contribute to the photocurrent.

The structure with  $R_o = 30$  produces the highest current. However, it is well known that the lower  $R_o$  values increase the SRO conductivity, so if the current goes through the SRO, the more conductive structure will be that with  $R_o = 10$ . On the other hand, it is also known that silicon excess of 5% (for  $R_o = 30$ ) produces the highest PL emission (Morales et al., 2005, Luna et al., 2009), and then the more sensible to radiation, where the PL (red emission) generates e-h pares in the induced PN junction. Then, these two mechanisms have to be further studied to determine which one is more adequate to improve the photoresponse of our sensor.

## 5. Conclusion

The influence of different factors on the structural (Si-nc, a-Si, Si-nanocluster, roughness) and optical properties (PL, absorption coefficients, optical band gap) of the SRO films has been discussed from experimental data. PL increased with the annealing time and decreased with a greater amount of silicon excess. In our case, it has been discussed that PL is not due to Si-ncs. Si-clusters are the main nanoparticles that produce maximum PL due to the different type of defects. The formation and growth of Si-ncs and the formation of a-Si in samples with different silicon excess after different annealing times were investigated with XRD and HRTEM. Interestingly, it was found that the optical band gap strongly correlates with the silicon excess and it is shifted over a large energy range via the reactants ratio.

These interesting properties of the SRO films were used to fabricate MOS-like structures, and an Al/SRO/Si MOS-like grid structure was fabricated and tested as photodetector. Silicon-rich oxide films with different silicon excesses were used as dielectric layers and deposited on silicon substrates of very high resistivity. This structure shows high optical sensitivity for the whole UV-Vis-NIR range. The high photocurrent results from three different components. One of them is due to photo-carriers generated in the SRO films; another one comes from the red light that is photo generated in the SRO, as mentioned above. This red light impinges into the high resistivity silicon producing electron-hole pairs. The third component comes from the electron-hole pairs generated in the silicon by the light absorbed in the silicon volume. In spite of the fact that the UV radiation produces electron-hole pairs near the silicon surface, they contribute to the photocurrent because there is not a death zone. Due to the high resistivity of the silicon a long diffusion length is obtained, and the photo generated minority carriers are able to reach the induced PN junctions under the Al grids.

## 6. Acknowledgment

This work has been partially supported by CONACyT-154725, PROMEP-231 and VIEP-BUAP-2011. The authors acknowledge technicians of INAOE laboratory for their help in the samples preparation and measurements.

## 7. References

- Aceves, M., O. Malik, V. Grimalsky, Application of silicon Rich Oxide Films in New Optoelectronic Devices, *Physics and Chemistry of Solid State* 2004, 5(2), pp. 234-240.
- Aceves, M., W. Calleja, C. Falcony, J. A. Reynoso-Hernández, The Al/Silicon Rich Oxide/Si P-N Induced Junction As A Photodetector, *Revista Química Analítica*, 1999, 18, 102.
- Ashkan, B.; Jason, J.; Yongho, C.; Leila, N.; Gunham, M.; Wu, Z.; Andrew, G.; Kapur, P.; Kriehna, C. & Ant, U. (2008). Metal-Semiconductor-metal photodetectors based on single-walled carbon nanotube film-GaAs Schottky contacts, *J. Appl. Phys.*, Vol.13, (June 2008), pp. 114315, ISSN 0021-8979
- Berman D. M., M. Aceves-Mijares, L. R. Berriel-Valdos, J. Pedraza, A. Vera-Marquina, Fabrication, characterization, and optimization of an ultraviolet silicon sensor, *Optical Engineering*, 2008, 47(10), 104001.
- Chen Y., T. Cheng, . Cheng, C. Wang, C. Chen, C. Wie, Y. Chen, Highly sensitive MOS photodetector with wide band responsivity assisted by nanoporous anodic aluminum oxide membrane, *Optics Express* 2010, 18(1), pp. 56-62.
- Comedi, D., O.H.Y. Zalloum, E. A. Irving, J. Wojcik, T. Roschuk, M. J. Flynn, and P. Mascher, X-Ray-Diffraction study of crystalline Si nanocluster formation in annealed silicon-rich silicon oxides, *J. Appl. Phys.* 99, 023512 (2006).
- Comedi, D., Zalloum, O.H.Y., Irving, E. A., Wojcik, J., Roschuk, T., Flynn, M. J., and Mascher, P., (2006), X-Ray-Diffraction study of crystalline Si nanocluster formation in annealed silicon-rich silicon oxides, *J. Appl. Phys.* 99, 023512 (2006), ISSN 0021-8979
- Di Maria, D. J., Kirtley, J. R., Pakulis J., Dong, D. W., Kuan, D., Pesavento, F. L., Theis, T. N., Cutro, N., Brorson, S. D.; (1984). Electroluminescence studies in silicon dioxide films containing tiny silicon islands, *J. Appl. Phys.*, Vol. 56(2) (1984), pp. 401-416, ISSN 0021-8979.
- DiMaria, D. J., Dong, , Pesavento, D. W., F. L.; Enhanced conduction and minimized charge trapping in electrically alterable read-only memories using off-stoichiometric silicon dioxide films, *J. Appl. Phys.*, 1984, 55(8), pp. 3000-3019, ISSN 0021-8979.
- Donald C., Cronmeyer, Hall and Drift Mobility in High-Resistivity Single-Crystal Silicon, *Phys. Rev.*, 1957, 105(2), 522.
- Foster J., J. K. Doyle, P. Mascher, A. P. Knights, and P. G. Coleman, Optical attenuation in defect-engineered silicon rib waveguides, *J. Appl. Phys.*, 2006, 99, pp. 073101, ISSN 0021-8979.
- Grove, A. S., *Physics and technology of semiconductor devices*, John Wiley and sons, USA 1967.



- Harkonen, J., E. Tuovinen, Z. Li, P. Luukka, E. Verbitskaya, V. Eremin, Recombination lifetime characterization and mapping of silicon wafers and detectors using the microwave photoconductivity decay (mPCD) technique, *Materials Science in Semiconductor Processing*, 2006, 9, 261.
- Hwang, J. & Lin, C. (2005). Gallium nitride photoconductive ultraviolet sensor with a sputtered transparent indium-tin-oxide ohmic contact, *Thin Solid Films*, Vol.491 (May 2010), pp. 276-279, ISBN 842-6508-233.
- Jørgensen, J. F., *The Scanning Probe Image Processor (SPIP)*, Denmark, 2002, [www.imagemet.com](http://www.imagemet.com).
- Karunakaran, B., Rajendra, R. T., Mangalaraj, D., Narayandass, K., Mohan, G., (2002), Influence of thermal annealing on the composition and structural parameters of DC magnetron sputtered titanium dioxide thin films, *Cryst. Res. Technol.*, Vol. 37 (12), 2002, pp. 1285-1292.
- Luna López, J. A., A. Morales Sanchez, M. Aceves-Mijares, Z. Yu, C. Dominguez, Analysis of surface roughness and its relationship with photoluminescence properties of silicon-rich oxide films, *J. Vac. Sci. Technol. A*, 2009, 27(1), 57.
- Luna-López, A., M. Aceves-Mijares, O. Malik, R. Glaenger, Low-and high-resistivity silicon substrate characterization using the Al/silicon-rich oxide/Si structure with comparison to the metal oxide semiconductor technique, *J. Vac. Sci. Technol. A*, 2005, 23 (3), 534-538.
- Luna-López, J. A., Aceves M., O. Malik, Z. Yu, A. Morales, C. Dominguez and J. Rickards, *Revista Mexicana de Física*, S 53(7), 293 (2007).
- Luna-López, J. A., M. Aceves-Mijares and O. Malik, Optical and electrical properties of silicon rich oxide films for optical sensor, *Sensors and actuators A*, 2006, 132, 278.
- Luna-López, J. A., M. Aceves-Mijares, A. Morales-Sánchez, J. Carrillo-López, Photoconduction in silicon rich oxide films obtained by LPCVD, *J. Vac. Sci. Technol. A* 28(2), Mar/ Apr 2010.
- Morales A., J. Barreto, C. Domínguez, M. Riera, M. Aceves and J. Carrillo, (2005), Comparative study between silicon-rich oxide films obtained by LPCVD and PECVD, *Physica E: Low-dimensional Systems and Nanostructures*, 2007, 38(1), 54.
- Nayfeh, O. M., S. Rao, A. Smith, J. Therrien, and M. H. Nayfeh, Thin Film Silicon Nanoparticle UV Photodetector, *IEEE Photonics Technology Letters*, 2004, 16(8), 1927.
- Pankove, J. I., *Optical Processes in Semiconductors*, (Dover New York, 1975), Chap. 4-6.
- Sabnis, V. A., Demir, H. V., Fidaner, O, Zheng, J. F., J S Harris, D A B Miller, N Li, T C Wu, H T Chen, Y M Houn (2005), Intimate Monolithic Integration of Chip-Scale Photonics Circuits, *IEEE J. selected Topics in Quantum Electronics* 2005, 11(6), pp. 1255.
- Spinella C., C. Bongiorno, G. Nicotra, and E. Rimini, *Appl. Phys. Lett.* 87, 044102 2005.
- Sze, S. M., *Physics of semiconductor devices*, John Wiley and sons, USA, (2006).
- Torchynska, T. V., *J. Appl. Phys.* 92, 4019 2002.
- Yu Z., M. Aceves-Mijares, J. A. Luna Lopez, J. Deng, Nanocrystalline Si-based metal-oxide-semiconductor, *Proc. SPIE* 7381 2009, pp. 7381 1H.
- Yu Z., Mariano Aceves-Mijares, A. Luna-López, Enrique Quiroga and R. López Estopier, "Photoluminescence and Single Electron Effect Of Nanosized Silicon Materials". In:

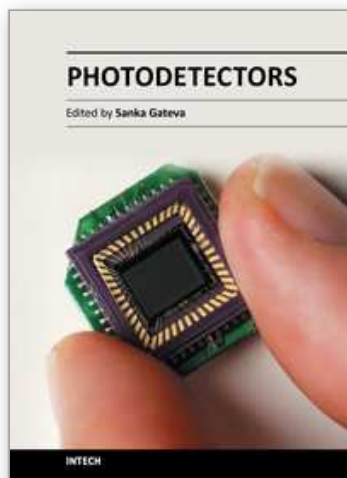


Focus on Nanomaterials Research, Editor: B. M. Carota, ISBN 1-59454-897-8 Nova Science Publishers, Inc., 2008, 233.

Yu, Z., M. Aceves-Mijares, K. Monfil, R. Kiebach, R. Lopez-Estopier, J. Carrillo, Room temperature current oscillations in naturally grown silicon nanocrystallites embedded in oxide films, J. Appl. Phys., 2008, 103, 063706.

IntechOpen

IntechOpen



## **Photodetectors**

Edited by Dr. Sanka Gateva

ISBN 978-953-51-0358-5

Hard cover, 460 pages

**Publisher** InTech

**Published online** 23, March, 2012

**Published in print edition** March, 2012

In this book some recent advances in development of photodetectors and photodetection systems for specific applications are included. In the first section of the book nine different types of photodetectors and their characteristics are presented. Next, some theoretical aspects and simulations are discussed. The last eight chapters are devoted to the development of photodetection systems for imaging, particle size analysis, transfers of time, measurement of vibrations, magnetic field, polarization of light, and particle energy. The book is addressed to students, engineers, and researchers working in the field of photonics and advanced technologies.

### **How to reference**

In order to correctly reference this scholarly work, feel free to copy and paste the following:

J.A. Luna-López, M. Aceves-Mijares, J. Carrillo-López, A. Morales-Sánchez, F. Flores-Gracia and D.E. Vázquez Valerdi (2012). UV-Vis Photodetector with Silicon Nanoparticles, Photodetectors, Dr. Sanka Gateva (Ed.), ISBN: 978-953-51-0358-5, InTech, Available from: <http://www.intechopen.com/books/photodetectors/uv-vis-photodetector-with-silicon-nanoparticles->

**INTech**  
open science | open minds

### **InTech Europe**

University Campus STeP Ri  
Slavka Krautzeka 83/A  
51000 Rijeka, Croatia  
Phone: +385 (51) 770 447  
Fax: +385 (51) 686 166  
[www.intechopen.com](http://www.intechopen.com)

### **InTech China**

Unit 405, Office Block, Hotel Equatorial Shanghai  
No.65, Yan An Road (West), Shanghai, 200040, China  
中国上海市延安西路65号上海国际贵都大饭店办公楼405单元  
Phone: +86-21-62489820  
Fax: +86-21-62489821

© 2012 The Author(s). Licensee IntechOpen. This is an open access article distributed under the terms of the [Creative Commons Attribution 3.0 License](#), which permits unrestricted use, distribution, and reproduction in any medium, provided the original work is properly cited.

IntechOpen

IntechOpen